

Role of in-medium hadrons in photon-nucleus reactions : shadowing and dilepton spectrum

Jan-e Alam^a, Sanjay K. Ghosh^b, Pradip Roy^c, Sourav Sarkar^a

^a Variable Energy Cyclotron Centre, 1/AF, Bidhannagar, Kolkata 700 064, INDIA

^b Department of Physics, Bose Institute, 93/1, A. P. C. Road, Kolkata 700 064, INDIA

^c Saha Institute of Nuclear Physics, 1/AF, Bidhannagar, Kolkata 700 064, INDIA

We study the effect of in-medium hadronic properties in photon nucleus interactions in the context of shadowing as well as the dilepton spectrum for incident photon energies in the range 1.1- 3 GeV. A reasonable agreement with the experimental data for shadowing is obtained in a scenario of downward spectral shift of the hadrons. We show that distinguishable features for in-medium changes of the hadronic properties can be observed experimentally through the dilepton spectrum by judicious choice of target nuclei and incident energy of photons.

I. INTRODUCTION

The study of in-medium properties of hadrons has been a field of great interest for quite some time. The recent renewed interest in this area of physics is mainly due to various results available from relativistic heavy ion collision experiments performed at the Super Proton Synchrotron at CERN and Relativistic Heavy Ion Collider at Brookhaven National Laboratory. Particularly a series of studies by the CERES/NA45, HELIOS-3 and NA50 collaborations at SPS with S+Au, S+W, Pb+Au and Pb+Pb collisions have largely been interpreted as the indication of a downward shift of the ρ^0 mass in the nuclear medium [1,2]. The invariant mass spectrum for dilepton production shows a large enhancement at low invariant mass regions. These excess dileptons are thought to originate from the decay of vector mesons with reduced mass [3,4] in the medium.

In a contrasting view, some authors explained this enhancement as a manifestation of the broadening of the ρ spectral function due to its coupling with baryonic resonances [5–7]. It was initially suggested that the drop in ρ mass is mainly governed by the chiral symmetry restoration. But in a theoretical study, combining chiral SU(3) dynamics with Vector Meson Dominance (VMD), it was shown that the chiral restoration does not demand a drastic reduction of vector meson mass in the nuclear medium [8]. This model also predicted a substantial broadening of ρ^0 spectral density with only a marginal mass reduction. In ref. [9–11] it was shown that in a non-chiral model like Walecka model a drastic reduction in ρ meson mass may be realized.

Presently the heavy ion experiments and the corresponding theoretical studies remain inconclusive mainly due to the fact that the medium effects here are masked by the complicated dynamics both in the initial as well as the final state. Moreover, the huge multiplicities and background makes it difficult to analyze the experimental data unambiguously.

The hadron-nucleus collisions [12], though seem to be less complicated compared to A-A collisions, will also suffer from the problem of initial as well as final state interactions. On the other hand, these difficulties are largely overcome with the use of photons which do not have the problem of initial state interaction. The high flux photon beam, which has compensated for the low interaction cross section with nuclear matter, complimented by wide angle multiparticle spectrometers, have made possible a new generation of experiments.

Detection of dileptons in experiments simplifies the problem further since in contrast to hadronic, dileptonic decay modes in nuclear matter are disturbed by the final state interaction. The small cross section for secondary interactions of the outgoing electrons with nuclear matter makes the dileptons an ideal probe for studying the reactions inside the nucleus.

The dominant feature of photon interaction above π production threshold with $0.14 < E_\gamma$ (GeV) < 0.5 , E_γ being the incident photon energy in GeV, is the Δ resonance production. Above this, in the range $0.5 < E_\gamma$ (GeV) < 1 , photon nucleus interaction can mainly be described by baryon resonance production. The $\gamma - A$ cross section per nucleon is suppressed compared to the $\gamma - N$ cross section in this energy range. Beyond ~ 1 GeV vector meson production becomes dominant and VMD is generally used to describe the interaction in this region.

In the present paper we confine our study in the region $1 < E_\gamma$ (GeV) < 3 to understand the role of in medium hadrons in shadowing as well as in the dilepton spectrum from γ -A reaction. Our endeavour to study shadowing as well as dilepton spectrum is important due to following reasons.

Firstly, the photo-nuclear data at low photon energies for different nuclei seem to indicate an early onset of shadowing [13,14]. This phenomena has been interpreted as a signature for lighter ρ meson in the nuclear medium [15]. In contrast,

the authors in ref. [16] have claimed that the early onset of shadowing can be understood within simple Glauber theory [17–20] if one takes the negative real part of the ρ -N scattering amplitude into account which corresponds to higher in-medium ρ mass. In [21], authors have concluded that the enhancement of shadowing at low energies occur mostly due to lighter ρ meson as well as intermediate π^0 produced in non-forward scattering.

But the situation is rather more involved as we have shown in our earlier work [22]. There are several factors which might contribute to the mismatch of theory and experiment. Glauber model, which was originally developed for high energy scattering, might be improved by taking care of the approximations inherent in it. Furthermore, improved estimate of the parameters of the Glauber model as well as multiple scattering, namely cross section/scattering amplitudes, might be able to give a better fit to the experimental data. In Ref. [22] we have addressed all these related problems to show that a good description of photoabsorption data is not unambiguous and there are some serious constraints in the proper understanding of the experimental results. On the other hand, if the dropping vector meson mass is the cause of early onset of the shadowing, it should be observed in the dilepton spectrum at low energies as well. In fact, the theoretical analysis of the dilepton spectrum is intimately related to the shadowing, as the photon-nucleon cross section inside a nucleus has to be multiplied by the effective number of nucleons *i.e.* A_{eff} ($< A$, being the mass number) of the nucleus, as obtained from shadowing studies, to obtain the final photon-nucleus cross section. Hence a study of the dilepton spectrum might put some additional constraints on the shadowing. The dilepton study itself may be less ambiguous as a good description of photon-nucleon data gives *a-priori* justification of the models used.

Recently, a large reduction of ρ mass in the nuclear medium has also been reported by TAGX collaboration [23], inferred from the dipion spectrum. ρ meson is certainly the best candidate to study the medium effects since due to its short life time and decay length a large portion of the ρ^0 mesons produced will decay inside the nuclear medium. But the detection of dipion is disadvantageous as they suffer final state interactions. Though e^+e^- branching ratio is small, the absence of final state interactions makes the analysis easier. Of course, there will be a large background mainly coming from the QED processes like Bethe-Heitler [24], but these can be eliminated with suitable cuts in the final spectrum [25].

In the present paper, we have studied, the propagation of the produced vector meson inside the nucleus. The snapshots at different times help us to understand the microscopic dynamics in γ -A collisions. It also reveals the fact that ω and ϕ mesons in contrast to the ρ mostly decay outside the nuclear environment. The path length traversed by the vector meson gives a direct correspondence of the dilepton spectrum and the medium density at which it has decayed.

The energy range considered here is similar to the proposed experiment at CEBAF [26], where incoherent photoproduction of vector mesons would be studied, with deuterium, carbon, iron and lead as targets. Though, there have been theoretical studies of coherent photoproduction earlier, a detailed study with in-medium effects was lacking. The present work shows that even in coherent processes, the medium effects would show up in an appropriate kinematic window. Furthermore, as the Bethe-Heitler contribution can be suppressed with an energy cut on final dileptons, the results presented here will give a fair idea regarding the quantitative contribution from other coherent processes in the presence of in-medium hadrons.

The paper is organized as follows. In section II, we have described the phenomena of shadowing. Section III is devoted to the study of the propagation of vector mesons inside the nucleus and their decay to lepton pairs. Finally in section IV we present summary and discussions.

II. SHADOWING IN PHOTOABSORPTION

The photonuclear cross section has been found to be suppressed compared to the photon-nucleon interaction for photon energies, $E_\gamma > 1$ GeV. This phenomenon is attributed to the phenomena of the nuclear shadowing. Here we would like to consider photon energies above 1 GeV where the the dominant process is the production of vector mesons in the initial state and the main tool for theoretical description is VMD.

A. Shadowing in γ -A reaction

If a photon impinges on a nucleus then, one would naively expect that the nucleus being transparent to the photon each nucleon will have equal probability to interact with the beam. In such a case the total cross section for γ -A reaction would be given by

$$\sigma_{\gamma A} = A\sigma_{\gamma N} \tag{1}$$

On the other hand, if the photon interacts with nucleus through its hadronic components, then, just like hadron-nucleus interaction, the photon's initial interaction will be principally with nucleons in the incoming side of the nucleus [27]. The nucleons further along the photon trajectory do not contribute to the total cross section. Hence the total cross section is expected to be smaller compared to the previous case, *i.e.* $\sigma(A) < A\sigma_{\gamma-N}$. This phenomena, observed both in hadron-nucleus as well as γ -nucleus interactions, is generally known as shadowing. In case of γ -A collision, such a picture would be valid only if the hadronic components of the photon are long lived. This is quantified in terms of the coherent length described later. The effect of shadowing can be written as,

$$\frac{A_{eff}}{A} = \frac{\sigma_{\gamma A}}{A\sigma_{\gamma N}} = 1 + \frac{\delta\sigma_{\gamma A}}{A\sigma_{\gamma N}} \quad (2)$$

where $\sigma_{\gamma A} = A\sigma_{\gamma N} + \delta\sigma_{\gamma A}$ consists of the incoherent scattering of the photon from individual nucleons and a correction due to the coherent interaction with several nucleons. In the present section we will discuss the medium effects on shadowing in γ -A reactions in the frame work of Glauber formalism [17,18] and multiple scattering [21,28,29] along with VMD [30].

1. Kinematics and coherence length

We consider a photon of energy $E_{\gamma L}$ colliding with a nucleus at rest. The nucleons inside the nucleus move with a Fermi momenta p_F or energy $E_F = \sqrt{p_F^2 + m_N^{*2}}$, which is a function of space co-ordinate through the density $n(r)$. The photon energy in the nucleon rest frame then becomes,

$$E_\gamma = \gamma_F E_{\gamma L} (1 - \beta_F \cos \theta_L), \quad (3)$$

$\beta_F = p_F/E_F$ and θ_L being the angle between incident photon and the Fermi momenta. The total invariant energy s can then be written as,

$$\begin{aligned} s &= (p_\gamma + p_F)^2 \\ &= m_N^{*2} + 2\gamma_F m_N^* E_{\gamma L} (1 - \beta_F \cos \theta_L), \end{aligned} \quad (4)$$

where m_N^* is the effective nucleon mass inside the nucleus. The modification of hadronic masses in nuclear environment have been studied in different models [11,31–33]. In the present study we consider two possible approaches for the effective mass of the nucleon inside a nucleus: (i) universal scaling scenario (USS) [31] and (ii) Quantum Hadrodynamical Model (QHD) [34]. In case of (i) the hadronic masses (m_H), except those of pseudo-scalar mesons, vary with the nuclear density $n(r)$ as

$$\frac{m_H^*}{m_H} = 1 - 0.2x, \quad (5)$$

where $x = n(r)/n_0(r)$ and $n_0(r)$ is the normal nuclear matter density ($\sim 0.15 \text{ fm}^{-3}$).

In the QHD model the effective masses of nucleons and vector mesons are calculated using standard techniques of thermal field theory [35,10] and parametrized as a function of $n(r)$ as follows:

$$\frac{m_H^*}{m_H} = 1 + \sum_{j=1} a_j x^j. \quad (6)$$

For nucleons $a_1 = -0.351277$ and $a_2 = 0.0766239$; in case of ρ , $a_1 = -1.30966$, $a_2 = 1.78784$, $a_3 = -1.17524$ and $a_4 = 0.294456$ and finally for ω , $a_1 = -0.470454$, $a_2 = 0.313825$ and $a_3 = -0.0731274$. No medium effects on the ϕ meson is considered as it is expected to be small in QHD [36]. The total invariant energy available for γN scattering now depends on the position of the participating nucleon through the effective nucleon mass which in turn depends on the density, $n(r)$ or the Fermi momentum p_F .

The vector meson produced inside the nucleus will have an effective mass which will depend on the density of the nuclear medium as seen by the meson. A direct effect of these mass changes would be reflected in the coherence length. The coherence length or the formation length (l_c) is the length scale of the hadronic component of the photon inside the nucleus. In other words, this corresponds to the time scale of the fluctuation between the bare photon and the hadronic component of the physical photon. When l_c is small, the hadron mediated interaction may become indistinguishable from bare photon interaction and there will not be any shadowing. In the present case, l_c is a

function of the radial distance inside the nucleus. For the vector meson with effective mass m_V^* , the coherence length is,

$$l_c = \frac{1}{E_\gamma - \sqrt{E_\gamma^2 - m_V^{*2}}} \sim \frac{2E_\gamma}{m_V^{*2}}, \quad (7)$$

where E_γ itself depends on the position of the struck nucleon through Eq. (3) as mentioned before.

2. Multiple Scattering Formalism

The formalism for the multiple scattering is based on the optical theorem [28,37]. The nuclear photoabsorption cross section in terms of amplitudes (\mathcal{A}) of the multiple scattering of the projectile with the nucleons inside the nucleus can be written as [29],

$$\sigma_{\gamma A} = \frac{1}{2m_N k} \text{Im} \sum_{n=1}^A \mathcal{A}^{(n)} \quad (8)$$

where k is the momentum of the photon and n corresponds to the number of nucleons participating in each multiple scattering process. The $n = 1$ term, *i.e.*, $\mathcal{A}^{(1)}$ is the amplitude of forward scattering of a photon with one bound nucleon and corresponds to the incoherent part in Eq. (2). The n_{th} order scattering amplitude $\mathcal{A}^{(n)}$ corresponds to the process where the incoming photon produces a hadronic state X_1 at the first nucleon, X_1 propagates freely upto second nucleon where a hadronic state X_2 is produced which then propagates freely to the third nucleon. This process continues till the hadronic state X_{n-1} scatters into outgoing photon from n_{th} nucleon. The nucleus is assumed to stay in the ground state which means that there is no energy transfer to the n nucleons. Hence the momentum transfer to the n_{th} nucleon is

$$\vec{q}_n = - \sum_{i=1}^{n-1} \vec{q}_i \quad (9)$$

The expression for $\mathcal{A}^{(n)}$ is,

$$i\mathcal{A}^{(n)} = \frac{A!}{(A-n)!} \prod_{i=1}^{n-1} \left[\int \frac{d^3 q_i}{2m_N (2\pi)^3} \right] F(\vec{q}_1) \cdots F(\vec{q}_n) i\mathcal{V}^{(n)}(\{\vec{q}_i\}) \quad (10)$$

where

$$\begin{aligned} i\mathcal{V}^{(n)} &= \sum_{X_i} i\mathcal{M}_{\gamma X_i}(\vec{q}_1) \frac{i}{\nu^2 - (\vec{k} - \vec{q}_1)^2 - m_{X_1}^2 - \Pi_{X_1}(\nu^2 - (\vec{k} - \vec{q}_1)^2)} i\mathcal{M}_{X_1 X_2}(\vec{q}_2) \\ &\times \frac{i}{\nu^2 - (\vec{k} - (\vec{q}_1 + \vec{q}_2))^2 - m_{X_2}^2 - \Pi_{X_2}(\nu^2 - (\vec{k} - (\vec{q}_1 + \vec{q}_2))^2)} \\ &\times \cdots i\mathcal{M}_{X_{n-1} \gamma}(\vec{q}_n) \end{aligned} \quad (11)$$

m_{X_i} and Π_{X_i} denote the mass and the vacuum self energy of the intermediate hadronic state X_i . \mathcal{M}_{ab} corresponds to the invariant amplitude for the process $a + n \rightarrow b + n$ and $F(\vec{q}_i)$ is the nuclear form factor,

$$F(\vec{q}_i) = \frac{1}{A} \int d^3 x e^{i\vec{q}_i \cdot \vec{x}} n(\vec{x}) \quad (12)$$

where $n(\vec{x})$ denotes the nucleon number density. Under eikonal approximation and neglect of the width of the vector meson in the intermediate state the above formalism reduces to the Glauber's formula. In the present context, in order to understand the role of in-medium hadrons, we modify the Glauber's formula. The photon entering the nucleus at an impact parameter b produces a vector meson at position z_1 . Inside the nucleus, the coherence length l_c , in general, would be different at z_1 (l_{c1}) and z_2 (l_{c2}) as the different densities will yield different masses. The expression for the shadowing part of the cross section is then given by [19],

$$\begin{aligned}
\delta\sigma_{VA} &= \frac{g_V^2}{4\pi\alpha} \delta\sigma_{\gamma A} \\
&= \frac{1}{2kk_V} \int d^2b \int dz_1 \int dz_2 \exp \left[-\frac{1}{2} \int \sigma_{VN}(z') n(b, z') dz' \right] \\
&\times k_V(z_1) \sigma_{VN}(z_1) k_V(z_2) \sigma_{VN}(z_2) n^{(2)}(b, z_1, z_2) \\
&\times \left[(\alpha_V(z_1) \alpha_V(z_2) - 1) \cos \left(\frac{z_1}{l_{c1}} - \frac{z_2}{l_{c2}} \right) \right. \\
&+ \left. \frac{1}{2} \int_{z_1}^{z_2} \alpha_V(z') \sigma_{VN}(z') n(b, z') dz' \right) - (\alpha_V(z_1) + \alpha_V(z_2)) \\
&\times \sin \left(\frac{z_1}{l_{c1}} - \frac{z_2}{l_{c2}} \right) + \left. \frac{1}{2} \int_{z_1}^{z_2} \alpha_V(z') \sigma_{VN}(z') n(b, z') dz' \right) \Big], \tag{13}
\end{aligned}$$

where $\alpha_V = \text{Re}f_{VV}/\text{Im}f_{VV}$ is the ratio of the real to the imaginary part of the VN forward scattering amplitude [20]. σ_{VN} is the $V - N$ scattering cross section [20] and k_V is the wave vector of the vector meson. The attenuation of the vector meson amplitude is described by the exponential factor. We have included 2-body correlation in the two-particle density as [16], $n^{(2)}(b, z_1, z_2) = n(b, z_1)n(b, z_2)[1 - j_0(q_c|z_1 - z_2|)]$, where $q_c = 780$ MeV and j_0 is the spherical Bessel function. The theoretical results of our calculations have been compared with experimental data. The extraction of experimental numbers has been discussed in ref. [22].

In the present paper we have discussed the results of shadowing for Carbon (C) and lead (Pb) nuclei. Depending on the size of the nucleus we have used two different density distributions; for $A < 16$ the shell model density profile of Ref. [38] and for heavier nuclei ($A > 16$) the density profile from ref. [39] has been used. According to eq. (3), E_γ is a function of angle, θ_L for non-zero p_F . The results which are presented here have been averaged over all possible values of θ_L . We have found that the effect of Fermi momentum in the kinematics (through eq. (3)) is small.

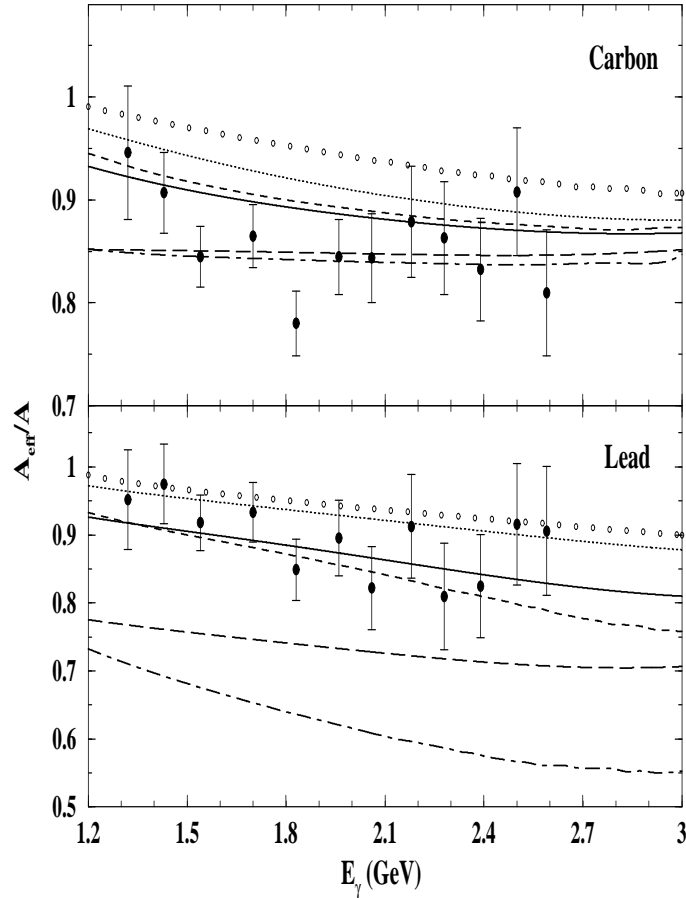


FIG. 1. A_{eff}/A for C and Pb nuclei as a function of photon energy. We show the results for both multiple scattering approach and Glauber model. The dotted, long-dashed and solid lines indicate calculations using Glauber model for vacuum, QHD and USS respectively. The circles, dot-dashed and short-dashed lines correspond to the same in the multiple scattering approach.

Fig. (1) shows the variation of A_{eff}/A with E_γ for C and Pb nuclei. We have used Glauber model and multiple scattering approach for the energy ranges considered here. We find that the USS gives a better description of the data both in the multiple scattering approach and Glauber model than the scenario with vacuum properties of hadrons. In QHD the drop of hadronic masses being larger, in general, the data is underestimated. On an average, our results show that the experimental data over the entire range of photon energy under consideration are reasonably well reproduced by the downward shift of the spectral function within the USS.

The results shown here have been found to be sensitive to the pole mass and largely insensitive to the broadening of the spectral function. But, more importantly, the results depends crucially on model (Glauber or multiple scattering) parameters, and less on the approximations (*e.g.* eikonal approximation) involved. Since the USS describe the data on shadowing reasonably well for the energy range $1 < E_\gamma$ (GeV) < 3 , we will evaluate the dileptons within this energy range in the USS. For comparison we will give results for both vacuum as well as QHD scenario.

III. DILEPTONS FROM γ -A COLLISION

The photoproduction of vector mesons, specifically ρ and ω mesons, have been studied before [40,41]. Recently dilepton spectrum have also been studied in photon-nucleus interaction using Boltzmann-Uheling-Uhlenbeck (BUU) formalism [42]. In this work we consider t channel processes (above resonance region) to study the effects of in-medium hadrons on the dilepton spectrum. The t channel diagrams considered in the present work provides a reasonable description of vector meson photoproduction data as we will show below (see also [41]). It is well known that to evaluate the lepton pair production from the leptonic decay of the vector meson in a nuclear medium all the processes which can either create or annihilate the vector meson under consideration has to be included in the imaginary part of its self energy (which is proportional to the in-medium width).

A. Coupling constants and form factors for t -channel processes

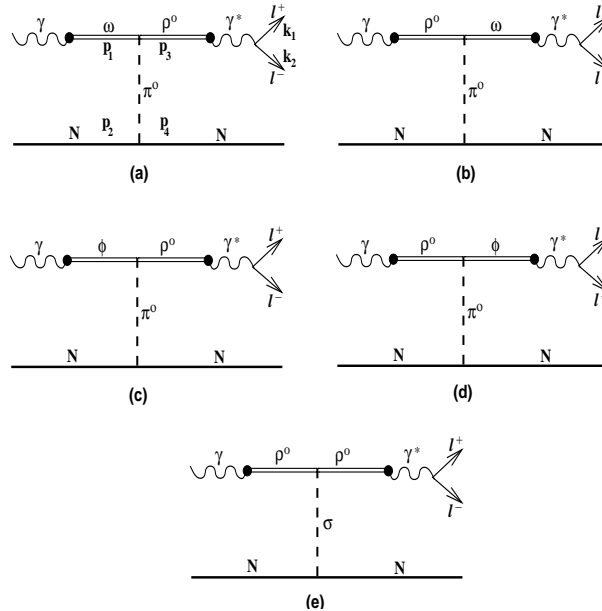


FIG. 2. Feynman diagrams for t -channel processes

Here we will describe the different processes and the evaluation of the required coupling constants. The reactions considered in this paper are shown in Fig. (2). The iso-scalar and iso-vector coupling of electromagnetic current and vector fields can be written following the current field identity [43]:

$$\begin{aligned}
\mathcal{J}_\mu^{(em)}(I=0) &= \frac{em_\omega^2}{g_\omega} \omega_\mu \\
\mathcal{J}_\mu^{(em)}(I=0) &= \frac{em_\phi^2}{g_\phi} \phi_\mu \\
\mathcal{J}_\mu^{(em)}(I=1) &= \frac{em_\rho^2}{g_\rho} \rho_\mu
\end{aligned} \tag{14}$$

where m_ω , m_ϕ and m_ρ are the masses of ω , ϕ and ρ mesons respectively. The couplings g_ω , g_ϕ and g_ρ are evaluated from the e^+e^- partial decay widths of the corresponding mesons and found to be 5.03, 13.25 and 17.05 respectively.

Processes (a)-(d) go through π and process (e) occurs via σ meson exchange. The exchange of vector mesons are not allowed because of the violation of charge conjugation invariance. The η exchange is not considered as it will be suppressed due to its larger mass and smaller value of coupling compared to pions. For the case of ω in the final channel, the neglect of η is further justified as $\omega \rightarrow \eta\gamma$ is two orders of magnitude lower than the $\omega \rightarrow \pi^0\gamma$. Due to opposite parity of π and σ , diagrams (a)-(d), which interfere among themselves, do not interfere with (e) [41]. The relative importance of π and σ exchange diagrams can be assessed from the radiative transition of vector mesons. The branching ratio of $\omega \rightarrow \pi^0\gamma$ is about an order of magnitude larger than that of $\omega \rightarrow \pi^+\pi^-\gamma$ which has an upper limit 3.6×10^{-3} [44] which implies a dominance of π exchange for ω in the final channel. In contrast, for ρ meson $\rho \rightarrow \pi^0\gamma$ is almost one order of magnitude lower than $\rho \rightarrow \pi^+\pi^-\gamma$ showing the importance of σ exchange over π for reactions involving ρ in the final channel.

Let us now consider the different interactions needed to evaluate the diagrams. The $\pi - N$ and $\sigma - N$ interactions are

$$\begin{aligned}
\mathcal{L}_{\pi NN} &= -ig_{\pi NN} \bar{N} \gamma_5 (\vec{\tau} \cdot \vec{\pi}) N \\
\mathcal{L}_{\sigma NN} &= g_{\sigma NN} \bar{N} N \sigma
\end{aligned} \tag{15}$$

where $g_{\pi NN} = 13.26$ and $g_{\sigma NN} = 10.03$ [41]. The corresponding vertex form factors are

$$F_{\pi NN} = \frac{\Lambda_{\pi(\sigma)}^2 - m_{\pi(\sigma)}^2}{\Lambda_{\pi(\sigma)}^2 - q^2} \tag{16}$$

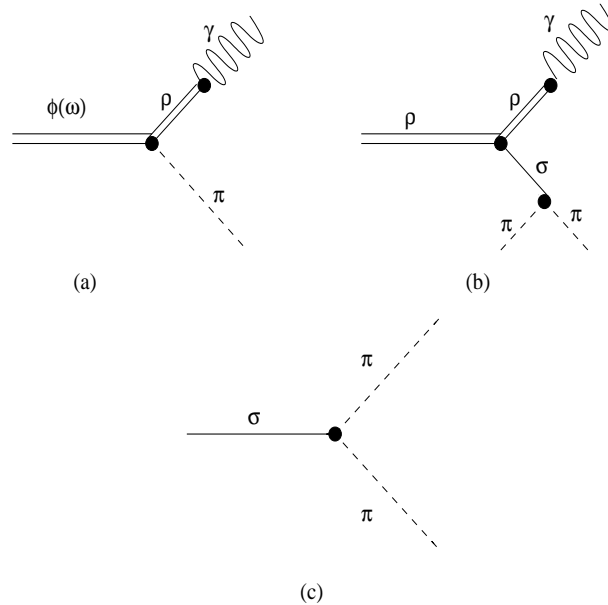


FIG. 3. Feynman diagram for coupling constants evaluation

The anomalous $\omega\rho\pi$ interaction [45] is given by

$$\mathcal{L}_{\omega\rho\pi} = \frac{g_{\omega\rho\pi}}{m_\pi} \epsilon^{\mu\nu\alpha\beta} \partial_\mu \omega_\nu \partial_\alpha \rho_\beta \pi. \tag{17}$$

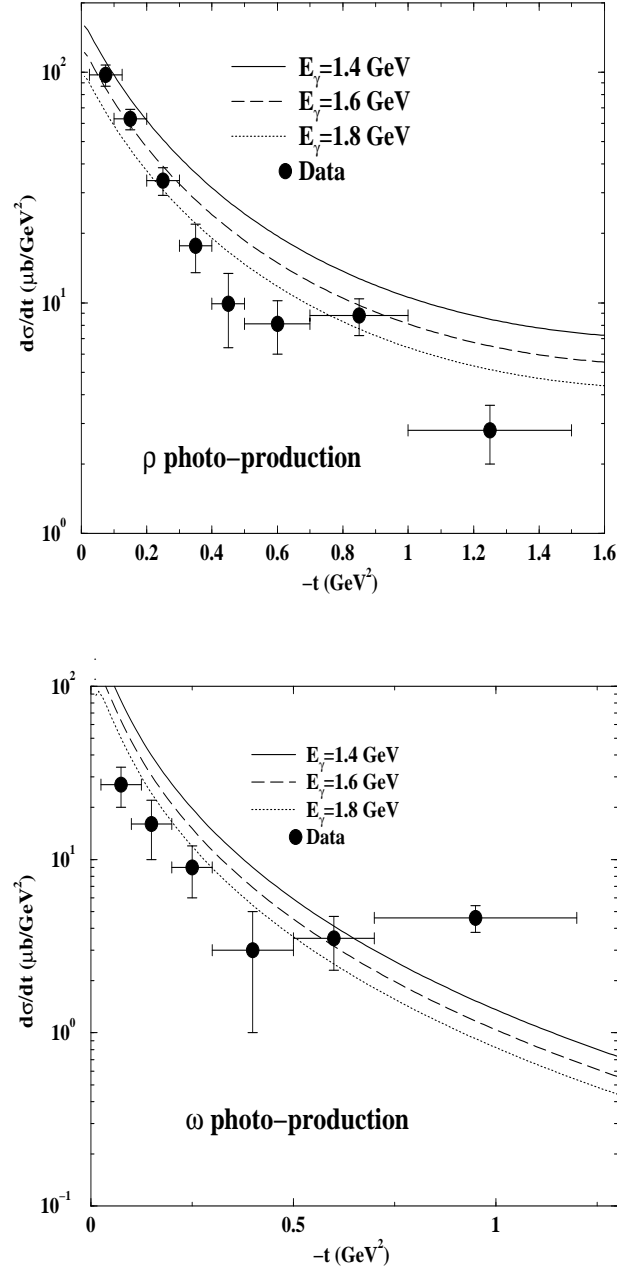


FIG. 4. ρ and ω photo-production cross-sections. The existing data is compared with the theoretical calculations (see [41] also).

The coupling constant $g_{\omega\rho\pi}$ is determined from the decay $\omega \rightarrow \pi^0 \gamma$ (see Fig. (3a)) assuming a ρ dominance. The decay width is given by

$$\Gamma_{\omega \rightarrow \pi^0 \gamma} = \frac{\alpha g_{\omega\rho\pi}^2}{24g_\rho^2} \frac{m_\omega^3}{m_\pi^2} \left(1 - \frac{m_\pi^2}{m_\omega^2}\right)^3 \quad (18)$$

We obtain $g_{\omega\rho\pi}$ to be 1.92 using $\Gamma_{\omega \rightarrow \pi^0 \gamma} = 715$ keV. The $\phi\rho\pi$ interaction can be written in a similar fashion. By using the radiative decay of ϕ , $g_{\phi\rho\pi}$ comes out to be 0.097.

The σ -exchange interaction for ρ photoproduction is given by

$$\mathcal{L}_{\sigma\rho\rho} = \frac{g_{\sigma\rho\rho}}{m_\pi} \partial^\alpha \rho^\beta (\partial_\alpha \rho_\beta - \partial_\beta \rho_\alpha) \sigma \quad (19)$$

The coupling constant $g_{\sigma\rho\rho} = 4.6$, is determined from $\rho \rightarrow \pi^+ \pi^- \gamma$ decay width given by (see Fig.(3b))

$$\Gamma_{\rho \rightarrow \pi^+ \pi^- \gamma} = \frac{\pi^2}{2m_\rho (2\pi)^5} \int dE_1 dE_2 \langle |\mathcal{M}|^2 \rangle \quad (20)$$

where E_1 and E_2 are the pion energies. The spin averaged matrix element squared is given by

$$\langle |\mathcal{M}|^2 \rangle = \frac{8\pi\alpha}{3} \frac{g_{\sigma\rho\rho}^2 g_{\sigma\pi\pi}^2}{g_\rho^2} m_\pi^2 \frac{(m_\rho - E_1 - E_2)^2}{[2m_\rho(E_1 + E_2) - m_\rho^2 - m_\sigma^2]^2}. \quad (21)$$

The coupling constant $g_{\sigma\pi\pi}$ is obtained as (see Fig. (3c))

$$g_{\sigma\pi\pi} = \frac{32\pi}{3} \frac{m_\sigma \Gamma_{\sigma \rightarrow \pi\pi}}{m_\pi^2} (1 - 4m_\pi^2/m_\sigma^2)^{1/2} = 17.6 \quad (22)$$

with $m_\sigma = 500$ MeV and $\Gamma_{\sigma \rightarrow \pi\pi} = 300$ MeV.

The $\sigma\rho\rho$ form factor in monopole form is given by,

$$F_{\sigma\rho\rho} = \frac{\Lambda_{\sigma\rho\rho}^2 - m_\sigma^2}{\Lambda_{\sigma\rho\rho}^2 - q^2} \quad (23)$$

The results for the differential cross sections of ρ and ω photoproduction in γ -nucleon collisions along with the experimental data for γ energy 1.4-1.8 GeV are shown in Fig. (4). The cut-off $\Lambda_{\pi(\sigma)}$ characterizing the $\pi(\sigma)$ -nucleon vertex is 0.7 GeV (1 GeV) [41]. $\Lambda_{\sigma\rho\rho} = 0.9$ GeV is taken from [41].

B. Propagation of vector mesons inside nucleus

The vector mesons produced inside the nucleus take a finite time to travel through the nucleus. The modification in their width affects the probability of these mesons to decay inside the nucleus. To have a better understanding of this phenomenon, we have studied the propagation of vector mesons with time after they are produced.

The minimum photon energy required to produce a vector meson of mass M can be calculated as follows. The magnitude of the three momentum $|\vec{p}_3|$ of the vector meson produced in a γ -nucleon collision is,

$$|\vec{p}_3| = \frac{1}{2\sqrt{s}} \lambda^{1/2}(M^2, m_N^2, s) \quad (24)$$

where λ is the triangular function defined in the appendix A. Substituting $s = m_N^2 + 2m_N E_\gamma$ in the above equation we obtain the threshold for the incident beam energy of the photon as $E_0 = M^2/2m_N + M$. For the production of ρ meson of mass 770 MeV $E_0 = 1.1$ GeV. It should be mentioned here that if the mass of the ρ reduces in the medium then this threshold will also reduce. For $E_0 = 1.1$ GeV the ρ mesons will be produced but not ω and ϕ . Therefore, any interference effects between ρ and ω will be absent. Moreover, for this incident photon energy the ρ will be created almost at rest so that it decays inside the nucleus. This will lead to a very clear signal for the shift of the ρ spectral function in the medium.

Now we will describe the methodology used to study vector meson propagation inside the medium. The matrix element for γ -N collision inside a nucleus would in general depend on the position r of the nucleon inside the nucleus. More specifically, the mass and width of the vector meson are functions of r inside the nucleus and is measured with respect to the center of the nucleus. The vector meson produced inside the nucleus at \vec{r} , would propagate inside the nucleus with a velocity \vec{v} (say) and would decay after traveling a distance given by $\vec{r}' = \vec{r} + \vec{v}t$ in time t . Now, the distance traveled by the vector meson would depend on its total decay width in the medium,

$$\Gamma_{\text{tot}} = \Gamma_0 + \Gamma_{\text{coll}}, \quad (25)$$

where Γ_0 is the decay width in vacuum and Γ_{coll} is the width due to the interaction of the vector meson in the medium. The increase in the width of the vector mesons reduce their life time in the medium and hence may allow them to decay within the nucleus. The time available to this vector meson to propagate, before it decays into dileptons, would be inversely proportional to Γ_{tot} . So one can now write the distance traveled $r_l = vt$ as,

$$r_l = \frac{\gamma v}{\Gamma_{\text{tot}}}; \quad \gamma = \frac{1}{\sqrt{1 - v^2}} \quad (26)$$

where the expression of v is,

$$v = \frac{|\vec{p}_3|}{E_3} = \sqrt{1 - \frac{4m_N^{*2}(r)M^2}{(s+t-m_N^{*2}(r))^2}} \quad (27)$$

where all the quantities in Eq. (27) are evaluated at the density of the production point r . The point at which the final vector meson decays can now be defined as,

$$r' = \sqrt{r^2 + r_l^2 - 2rr_l \cos \theta} \quad (28)$$

θ being the angle between the velocity vector \vec{v} and \vec{r} .

The vector meson passing through the nucleus may undergo multiple collisions with the other particles present in the medium which leads to a broadening of its width, which can be estimated in following manner [46]. Assuming that the vector meson is narrow and medium density is rather low, the intensity of the vector mesons passing through the vacuum can be described as,

$$|\psi(t_{life})|^2 = |\psi(0)|^2 e^{-\frac{\Gamma_0 t_{life}}{\gamma}} \quad (29)$$

In the nuclear medium this intensity decreases further due to scattering and absorption processes. In the medium Γ_0 is replaced by Γ_{tot} which is given by Eq. (25). So the net reduction would go as $\exp(-\Gamma_{tot} t_{life}/\gamma)$. The increase in width due to collisional broadening in the medium is given by,

$$\Gamma_{coll} = n(r)\sigma^* v \gamma \quad (30)$$

where σ^* is the total vector meson - nucleon cross section and $n(r)$ is the density of the nuclear medium. The average number of collisions the vector meson suffers in the medium can be estimated to be 3 for Pb and 1.6 for C at $E_\gamma = 1.1$ GeV. For $E_\gamma = 2$ GeV these numbers are 3 and 1.6 respectively. These clearly show that number of collisions is not very large, even for Pb. In that case, the experimental picture, perhaps will be closer to the no broadening scenario. Mass modifications in the medium appears to be the major factor in this case.

C. Dilepton spectrum

The formalism discussed in previous sections have been used to evaluate γ -A cross section for different scenarios. Here we would like to point out that at low energies some of the baryonic resonances get coupled to the ρ meson. It has been shown in [47] that these couplings make the ρ spectral function very broad. In the present work this effect is taken into account through the width of the spectral function. To avoid double counting one should not separately add dilepton production from these resonances as these are already included in the spectral function [48].

Now the matrix element for dilepton production (Fig. 2) is recasted so as to incorporate the co-ordinate dependence for production and decay points. For a reaction of the type $p_1 + p_2 \rightarrow p_3 + k_1 + k_2$ this is generically given by,

$$|\mathcal{M}|^2 = \mathcal{A}_{ex} \frac{(k_1 \cdot k_2) [(p_1 \cdot k_1)^2 + (p_1 \cdot k_2)^2] (p_2 \cdot p_4 + m_N^2(r))}{[m_{p_1}^4(r) + m_{p_1}^2(r)\Gamma_{p_1}^2(r)] [(M^2 - m_{p_3}^2(r'))^2 + m_{p_3}^2(r')\Gamma_{p_3}^2(r')] [(t - m_{ex}^2(r))^2 + \Gamma_{ex}^2(r)m_{ex}^2(r)]} \quad (31)$$

where m_{ex} and Γ_{ex} are the mass and decay width of the exchanged particles (π and σ in the present case). The masses of the initial state vector mesons (m_{p_1}) produced via VMD and the nucleon mass m_N depend on r whereas mass m_{p_3} and width Γ_{p_3} , for the final vector mesons are evaluated at r' . \mathcal{A}_{ex} contains all the factors coming from the different couplings (see appendix B). The effective masses are evaluated using Eq. (5) for universal scaling and Eq. (6) for QHD scenarios. The 4-momenta p_1, p_2, p_3 , and p_4 correspond to the initial photon, initial nucleon, intermediate vector meson and final nucleon respectively. The vector meson with momentum p_3 finally decays to lepton pairs of momenta k_1 and k_2 via a virtual photon. The differential cross section for such a process can be written as (see Appendix for details),

$$\frac{d\sigma_{l+l-}}{dM^2} = \frac{1}{256\pi^3\lambda(s, 0, m_N^2)} \int_{t_{1min}}^{t_{1max}} \frac{dt_1}{\lambda^{1/2}(M^2, 0, t_1)} \int_{t_{2min}}^{t_{2max}} dt_2 |\overline{\mathcal{M}}(M^2, t_1, t_2)|^2 \quad (32)$$

The detailed forms of the matrix elements \mathcal{M} are given in the appendix along with the expressions as well as allowed regions of s , t_1 and t_2 . In order to incorporate medium effects on the dilepton cross-section from $\gamma - A$ collisions we convolute the above equation with the density profile of the nucleus concerned. As mentioned earlier, there is

shadowing phenomenon in $\gamma - A$ reactions which affects the dilepton production. Taking these facts into account we obtain dilepton production cross-section per nucleon from $\gamma - A$ reactions as

$$\frac{d\sigma_{l^+l^-}^A}{dM^2} = \frac{1}{256\pi^3\lambda(s, 0, m_N^2)} \frac{\int d^3r \rho(r) \int_{t_{1min}}^{t_{1max}} \frac{dt_1}{\lambda^{1/2}(M^2, 0, t_1)} \int_{t_{2min}}^{t_{2max}} dt_2 |\overline{\mathcal{M}}(M^2, t_1, t_2)|^2}{\int d^3r \rho(r)} \quad (33)$$

The invariant mass distribution of the lepton pairs resulting from the decay of the vector meson *inside* the nucleus is given by

$$\frac{d\sigma_{l^+l^-}^{in}}{dM^2} = \frac{\int (1 - P(R_A)) \frac{d\sigma_{l^+l^-}}{dM^2} \rho(r) d^3r}{\int \rho(r) d^3r} \quad (34)$$

where $P(R_A)$ is given by,

$$P(R_A) = e^{-MR_A\Gamma_{tot}/|p\vec{3}|} \quad (35)$$

is the probability of the vector mesons of mass M to decay outside the nuclear radius R_A . In a similar way one can evaluate the dilepton emission rate *outside* the nucleus by replacing $(1 - P(R_A))$ by $P(R_A)$ in Eq. (34).

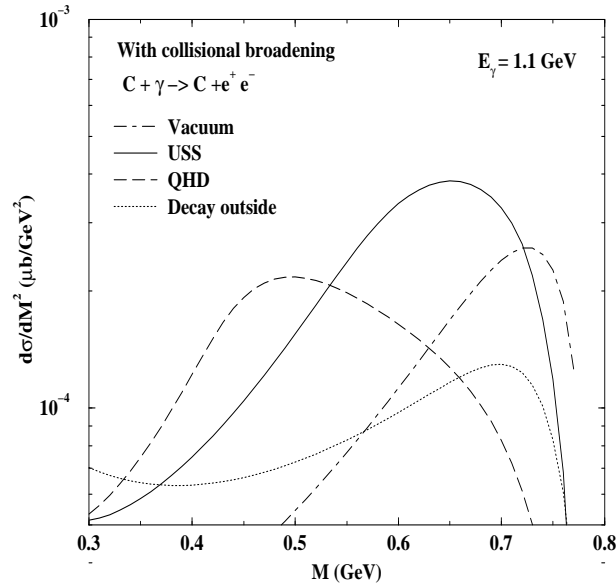


FIG. 5. Invariant mass distribution of lepton pairs from γ -C collisions at $E_\gamma = 1.1$ GeV. The result indicated by vacuum corresponds to the mass of the vector meson in vacuum and the in-medium width evaluated by using eq. 25. The curves denoted by USS and QHD correspond to the medium dependent masses given by eqs. 5 and 6 respectively.

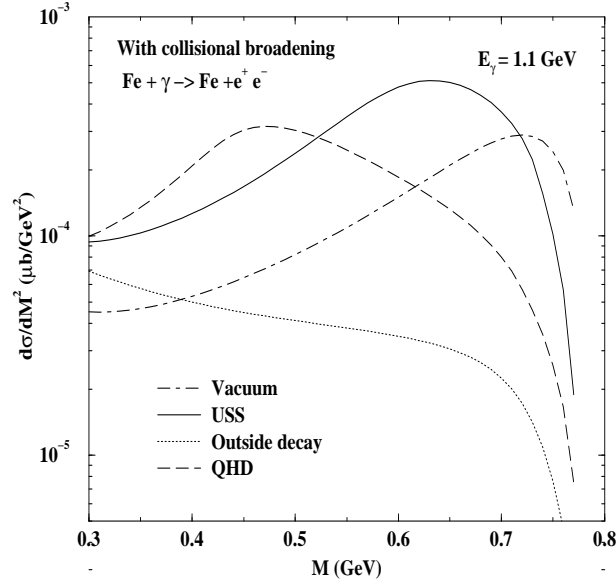


FIG. 6. Same as Fig.5 for γ -Fe collisions.

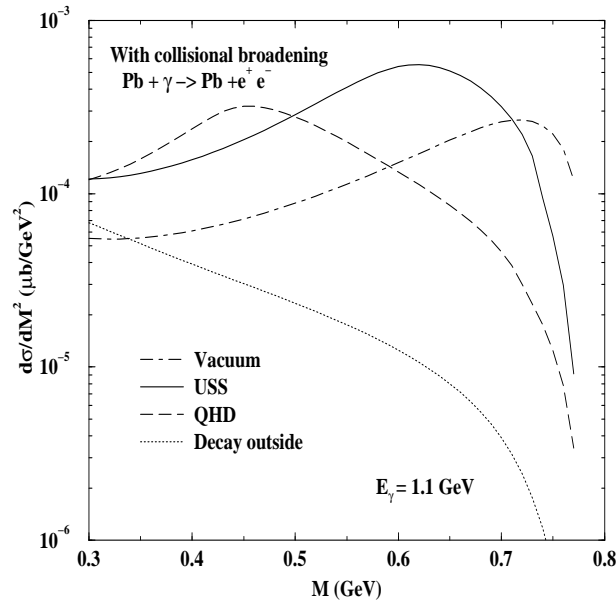


FIG. 7. Same as Fig.5 for γ -Pb collisions.

In Figs. 5, 6,7 we have depicted the the invariant mass distribution of lepton pairs for incident photon energy of 1.1 GeV for C, Fe and Pb nuclei respectively. $d\sigma/dM^2$ indicates the expected dilepton spectrum if the vector mesons decay inside or outside depending on the energy as well as their decay widths. If the meson decays outside, a sharp peak is to be observed at the ρ mass of 770 MeV. In the case of mesons decaying inside, one observes distinguishable differences between the vacuum and the in-medium scenarios. At $E_\gamma = 1.1$ GeV only the ρ meson can be produced with negligible velocity. In this case the probability for the decay of ρ inside the nucleus is maximum. Hence it will bring the information of the in-medium spectral function of the ρ most effectively. In the present case the width of the ρ due its interaction with baryonic resonances is given by Eq. (25) and the pole of the spectral function is shifted according to Eq. (5) or (6). For all the targets (C, Fe and Pb) considered here, the decay probability of the ρ meson outside the nucleus is much smaller than its decay inside. For incident photon energy close to the threshold the heavier the target less is the decay probability outside the nucleus. The effects of the in-medium modification of the ρ is clearly visible through dilepton spectra for the scenarios, *i.e.* USS and QHD for the entire range of M

considered here.

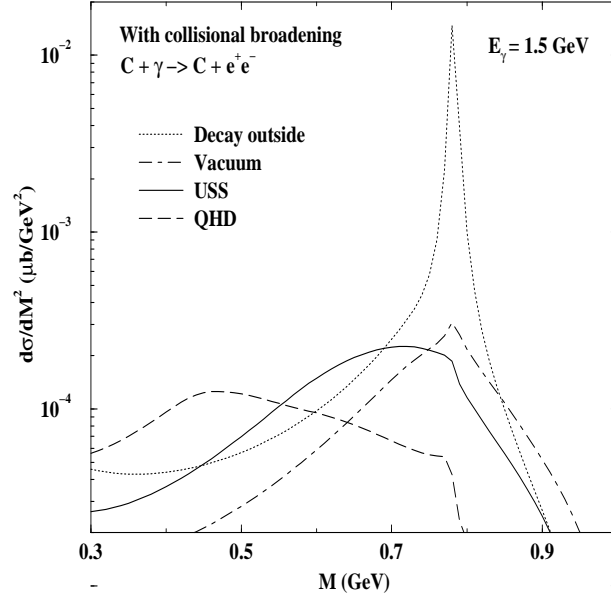


FIG. 8. Same as Fig.5 for $E_\gamma = 1.5 \text{ GeV}$.

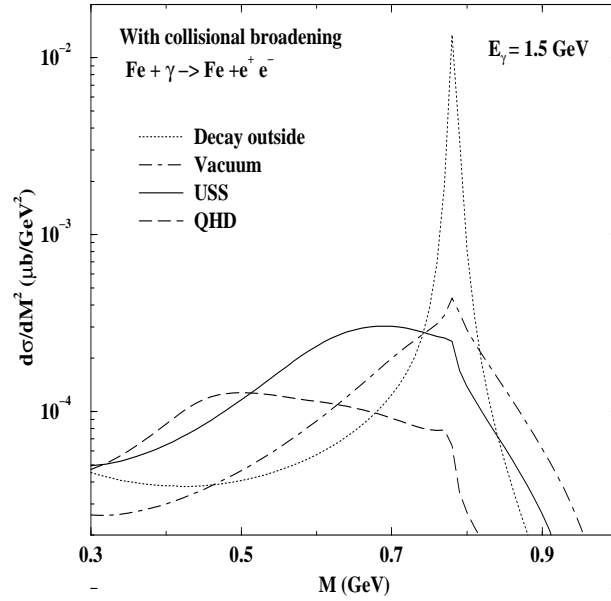


FIG. 9. Same as Fig.6 for $E_\gamma = 1.5 \text{ GeV}$.

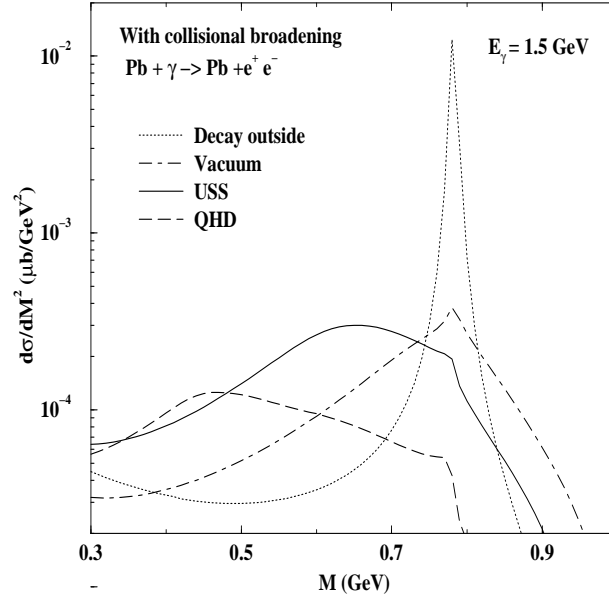


FIG. 10. Same as Fig.7 for $E_\gamma = 1.5$ GeV.

In Figs. 8, 9 and 10 we show the dilepton emission cross section as a function of the invariant mass, M for $E_\gamma = 1.5$ GeV. At this energy ρ and ω mesons may be created inside the nucleus with non-zero velocity. $E_\gamma = 1.5$ GeV is below the ϕ production threshold. The decay probability of the vector meson outside the nuclear volume increases with incident photon energy. For smaller nucleus (carbon, say) the dilepton spectra for the vector mesons decaying inside is marginally larger than the spectra originating from the decays outside for $M < 0.5$ GeV since the vector meson with non-zero velocity has a probability to traverse the (small) nucleus before decaying. However, for larger nuclei (Fe and Pb) the decay probability inside the nucleus is more. Consequently, the dilepton spectra from the vector mesons decaying inside dominates over the one corresponding to the decay outside for invariant mass region $0.3 < M(\text{GeV}) < 0.7$ for USS and QHD scenario.

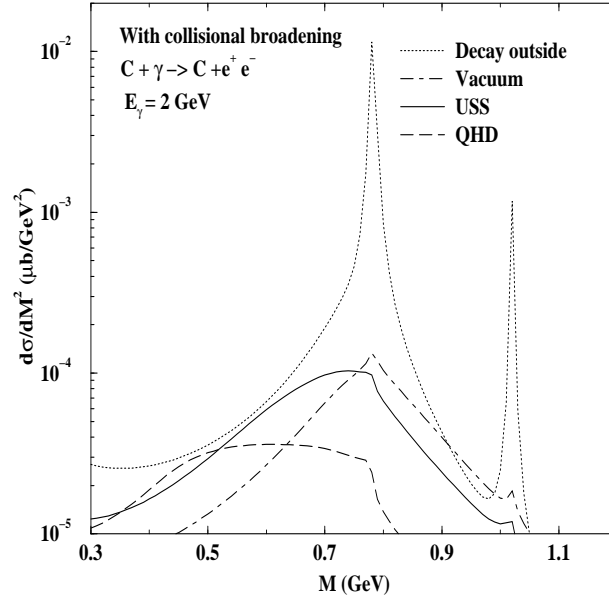


FIG. 11. Same as Fig.5 for $E_\gamma = 2$ GeV.

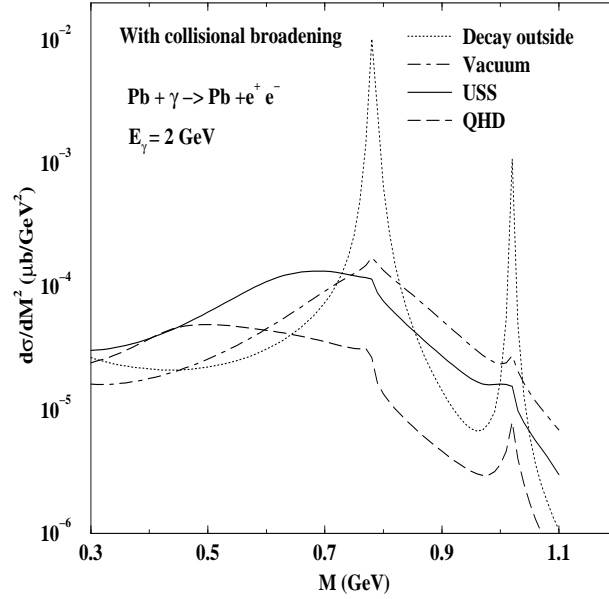


FIG. 12. Same as Fig.7 for $E_\gamma = 2$ GeV.

The dilepton spectra for $E_\gamma = 2$ GeV are shown in Figs. 11 and 12 for C and Pb respectively. At this energy all the three low mass vector mesons (ρ , ω and ϕ) are produced with finite velocity. They are likely to pass through the whole nucleus and decay outside. This is reflected in the invariant mass distribution of dileptons from carbon target, where most of the vector mesons decay outside the nuclear volume. In case of Pb target, however, the lepton pairs from vector mesons decaying inside dominates in the low invariant mass region.

In Figs. 13 and 14 we plot the invariant mass distribution of lepton pairs as a function of the path length traveled by the vector mesons inside the nucleus for $E_\gamma = 1.1$ and 2 GeV respectively. The path length of the vector meson can be calculated by using the equation $l = \frac{|\vec{p}_3|}{M} / \Gamma_{tot}$. This has been averaged over the Mandelstam variable t (contained in p_3). l indicates the distance inside the nucleus probed by the vector meson. In view of the fact that at a given nuclear density the ρ is lighter in QHD than USS, it is clear from the results shown in Figs. 13 and 14 that lighter the mesons the more it penetrates the target.

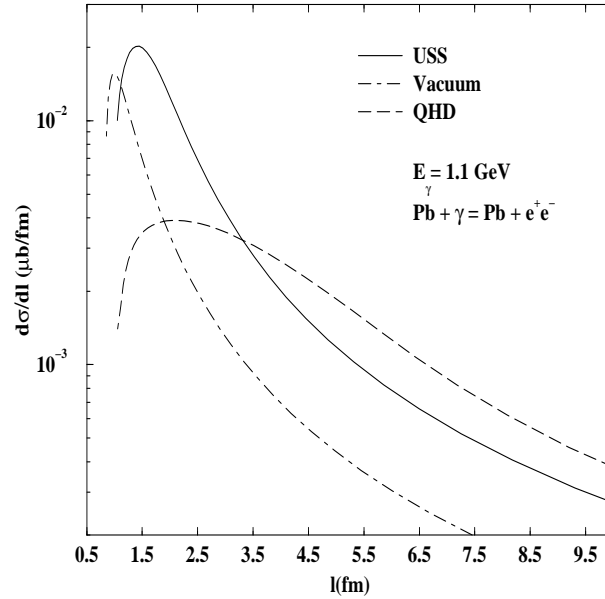


FIG. 13. The dilepton spectra as a function of average path length inside the Pb nucleus for $E_\gamma = 1.1$ GeV.

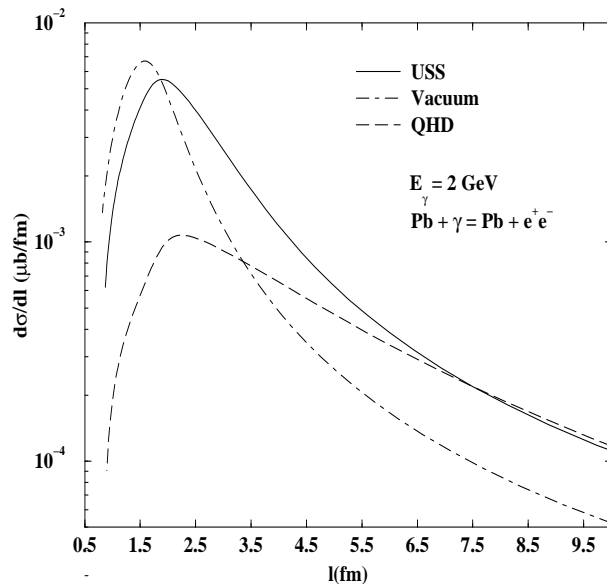


FIG. 14. The dilepton spectra as a function of average path length inside the Pb nucleus for $E_\gamma = 2$ GeV.

IV. SUMMARY AND DISCUSSIONS

In this work we have studied the effects of the spectral shift of vector mesons on the photon-nucleus interactions. It is found that the experimental data on nuclear shadowing can be well described within the ambit of universal scaling scenario proposed by Brown and Rho. The spectral shift of vector mesons in Quantum Hadrodynamical model seems to underestimate the data. On the other hand vector mesons with their vacuum properties overestimate the data. However, we emphasize that our understanding of the shadowing phenomena vis-a-vis Glauber model may be improved through corrections to the approximations inherent in the model as well as by examining the model parameters critically. The leading correction to the Glauber model due to deviation from eikonal propagation gives rise to a correction $\sim (2P_{cm}^A R)^{-1}$ relative to the Glauber scattering amplitude [49]. Here P_{cm}^A is the centre of mass momentum of the nucleus and R is its charge radius. In the present case the correction is rather small for $E_\gamma > 1$ GeV. Moreover, a refinement of the Glauber model (multiple scattering) parameters, *e.g.*, vector meson-nucleon scattering amplitude, two nucleon correlation etc. might give a good agreement with the data even with the vacuum properties of the hadrons. Hence a better estimate of these quantities is essential for a definitive statement regarding the role of medium effects on shadowing in photo-absorption processes. Experimental data with better statistics would certainly help us to resolve these uncertainties.

We have shown that the modification of the hadronic spectral function inside the nucleus drastically change the invariant mass distribution of lepton pairs originating from the decays of the vector mesons. To bring out the effect of different densities and hence effective in-medium masses and widths, we have explicitly incorporated the co-ordinate dependence for production and decay points. The dilepton spectra originating from the vector meson decays show strong dependence on the incident photon energy and mass number of the target nuclei. For this purpose we have considered incident photon energies of 1.1, 1.5 and 2 GeV on carbon, iron and lead nuclei. It has been demonstrated that by tuning the incident photon energy one can create the vector meson inside the nucleus with very small velocity. This will facilitate it to decay within the nuclear volume and leptons being electromagnetically interacting particles should carry the information of the in-medium properties of the vector mesons very efficiently. We have also shown that heavier the nucleus more visible are the medium effects.

It is to be remembered that the “signal” for the modification of the vector mesons properties should be filtered out from the background from Dalitz decays and decay of the vector mesons outside the nucleus. By fixing the beam energy one can minimize the later contributions. For the estimation of the backgrounds from Dalitz decays one needs to know the distributions of the hadrons *e.g.* π , η , ω , Δ 's etc produced in γ -A collision. The contributions from Bethe-Heitler process can be eliminated by suitable cuts in the final spectra.

APPENDIX

A. Differential cross-section for $2 \rightarrow 3$ particle scattering

We treat the $2 \rightarrow 3$ scattering process on the basis of the factorization of the phase space integral into two processes $2 \rightarrow 2$ and $1 \rightarrow 2$. We choose the two-particle intermediate system to be $k_1 + k_2$. The differential cross-section for the process $p_1 + p_2 \rightarrow p_3(k_1 + k_2) + p_4$ is given by [50],

$$\sigma_{l+l^-} = \int \frac{|\overline{\mathcal{M}}|^2 d\text{Lips}}{\mathcal{F}}, \quad (\text{A.1})$$

where \mathcal{F} is the flux factor given by $\mathcal{F} = 2\lambda(s, m_1^2, m_2^2)$ with $\lambda(x, y, z) = x^2 + y^2 + z^2 - 2(xy + yz + zx)$. The Lorentz-invariant phase space factor is given by

$$\int d\text{Lips} = \int \frac{d^3 p_4}{(2\pi)^3 2E_4} \frac{d^3 k_1}{(2\pi)^3 2\omega_1} \frac{d^3 k_2}{(2\pi)^3 2\omega_2} (2\pi)^4 \delta^4(p_1 + p_2 - p_4 - k_1 - k_2). \quad (\text{A.2})$$

In order to write the intermediate state explicitly in the phase space integral, the identity

$$1 = \int ds_2 \int \frac{d^3 p_3}{2E_3} \delta^4(p_3 - k_1 - k_2) \quad (\text{A.3})$$

with $E_3^2 = \mathbf{p}_3^2 + s_2$ is used in Eq. (A.2) to obtain

$$\begin{aligned} \int d\text{Lips} &= \frac{1}{(2\pi)^5} \int s_2 \left\{ \int \frac{d^3 p_4}{2E_4} \frac{d^3 p_3}{2E_3} \delta^4(p_1 + p_2 - p_3 - p_4) \right\} \\ &\quad \times \left\{ \int \frac{d^3 k_1}{2\omega_1} \frac{d^3 k_2}{\omega_2} \delta^4(p_3 - k_1 - k_2) \right\} \\ &= \frac{1}{(2\pi)^5} \int ds_2 R_2(s, m_4^2, s_2) R_2(s_2, m_{k_1}^2, m_{k_2}^2), \end{aligned} \quad (\text{A.4})$$

where $s = (p_1 + p_2)^2$. Let us consider the first two particle phase space $R_2(s, m_4^2, s_2)$. Going to CMS: $\mathbf{p}_1 + \mathbf{p}_2 = 0$ one obtains

$$\begin{aligned} R_2(s, m_4^2, s_2) &= \frac{\pi}{2} \int \frac{p_4^2 dp_4 d\cos\theta_{24}}{4E_4 E_3} \delta(E_1 + E_2 - E_4 - E_3) \\ &= \frac{\pi}{2\sqrt{s}} p_{4\text{cm}} \int d\cos\theta_{24} \\ &= \frac{\pi}{2\lambda^{1/2}(s, m_1^2, m_2^2)} \int dt_1, \end{aligned} \quad (\text{A.5})$$

with $t_1 = (p_1 - p_3)^2 = (p_2 - p_4)^2 = m_2^2 + m_4^2 - 2E_2 E_4 + 2p_{2\text{cm}} p_{4\text{cm}} \cos\theta_{24}$.

The second two-particle phase space integral, in the rest frame of $\mathbf{k}_1 + \mathbf{k}_2$ (quantities denoted by R), can be written as

$$\begin{aligned} R_2(s_2, m_{k_1}^2, m_{k_2}^2) &= \int \frac{d^3 k_1}{4\omega_1 \omega_2} \delta(E_3 - \omega_1 - \omega_2) \\ &= 2\pi \frac{\lambda^{1/2}(s_2, m_{k_1}^2, m_{k_2}^2)}{8s_2} \int d\cos\theta_{k_1 p_1}^R \end{aligned} \quad (\text{A.6})$$

We define the invariant variable t_2 as follows:

$$t_2 = (p_1 - k_1)^2 = m_1^2 + m_{k_1}^2 - 2E_1^R \omega_1^R + 2p_1^R k_1^R \cos\theta_{k_1 p_1}^R \quad (\text{A.7})$$

so that $dt_2 = \lambda^{1/2}(s_2, m_1^2, t_1) \lambda^{1/2}(s_2, m_{k_1}^2, m_{k_2}^2) d\cos\theta_{k_1 p_1}^R / 2s_2$ and we obtain from Eq. (A.6)

$$R_2(s_2, m_{k_1}^2, m_{k_2}^2) = \frac{\pi}{2\lambda^{1/2}(s_2, m_1^2, t_1)} \int dt_2 \quad (\text{A.8})$$

Finally, combining Eqs. (A.1), (A.4), (A.5) and (A.8) the dilepton production cross-section is obtained as

$$\frac{d\sigma_{l+l-}}{dM^2 dt_1 dt_2} = \frac{|\overline{\mathcal{M}}(M^2, t_1, t_2)|^2}{256\pi^3 \lambda(s, 0, m_N^2) \lambda^{1/2}(M^2, 0, t_1)} \quad (\text{A.9})$$

The limits of t_1 and t_2 are given by

$$t_1|_{min}^{max} = 2m_N^2 - \frac{1}{2s} \left[(s + m_N^2)(s - M^2 + m_N^2) \mp \lambda^{1/2}(s, m_N^2, 0) \lambda^{1/2}(s, m_N^2, M^2) \right] \quad (\text{A.10})$$

$$t_2|_{min}^{max} = -\frac{1}{2}(M^2 - t_1) \pm \left[\lambda^{1/2}(M^2, 0, 0) \lambda^{1/2}(M^2, t_1, 0) \right] \quad (\text{A.11})$$

B. Invariant amplitudes

The invariant amplitudes for the Feynman diagrams shown in Fig. (2)(a-e) are given by

$$\mathcal{M}_a = \frac{-ieF_\pi g_{\gamma\omega} g_{\gamma\rho} g_{\pi NN} g_{\omega\rho\pi} \epsilon^{\mu\nu\alpha\beta} p_{1\mu} \epsilon_\nu^\gamma(p_1) (k_1 + k_2)_\alpha \bar{u}_l(k_2) \gamma_\beta v_l(k_1) \bar{u}_N(p_4) \gamma_5 u_N(p_2)}{M^2 m_\pi [t_1 - m_\pi^2] [m_\omega^2 - im_\omega \Gamma_\omega] [M^2 - m_\rho^2 + im_\rho \Gamma_\rho]} \quad (\text{A.12})$$

$$\mathcal{M}_b = \frac{-ieF_\pi g_{\gamma\rho} g_{\gamma\omega} g_{\pi NN} g_{\omega\rho\pi} \epsilon^{\mu\nu\alpha\beta} p_{1\mu} \epsilon_\nu^\gamma(p_1) (k_1 + k_2)_\alpha \bar{u}_l(k_2) \gamma_\beta v_l(k_1) \bar{u}_N(p_4) \gamma_5 u_N(p_2)}{M^2 m_\pi [t_1 - m_\pi^2] [m_\rho^2 - im_\rho \Gamma_\rho] [M^2 - m_\omega^2 + im_\omega \Gamma_\omega]} \quad (\text{A.13})$$

$$\mathcal{M}_c = \frac{-ieF_\pi g_{\gamma\phi} g_{\gamma\rho} g_{\pi NN} g_{\phi\rho\pi} \epsilon^{\mu\nu\alpha\beta} p_{1\mu} \epsilon_\nu^\gamma(p_1) (k_1 + k_2)_\alpha \bar{u}_l(k_2) \gamma_\beta v_l(k_1) \bar{u}_N(p_4) \gamma_5 u_N(p_2)}{M^2 m_\pi [t_1 - m_\pi^2] [m_\phi^2 - im_\phi \Gamma_\phi] [M^2 - m_\rho^2 + im_\rho \Gamma_\rho]} \quad (\text{A.14})$$

$$\mathcal{M}_d = \frac{-ieF_\pi g_{\gamma\rho} g_{\gamma\phi} g_{\pi NN} g_{\phi\rho\pi} \epsilon^{\mu\nu\alpha\beta} p_{1\mu} \epsilon_\nu^\gamma(p_1) (k_1 + k_2)_\alpha \bar{u}_l(k_2) \gamma_\beta v_l(k_1) \bar{u}_N(p_4) \gamma_5 u_N(p_2)}{M^2 m_\pi [t_1 - m_\pi^2] [m_\rho^2 - im_\rho \Gamma_\rho] [M^2 - m_\phi^2 + im_\phi \Gamma_\phi]} \quad (\text{A.15})$$

$$\mathcal{M}_e = \frac{-2eF_\sigma g_{\gamma\rho}^2 g_{\sigma\rho\rho} g_{\sigma NN} \epsilon_\mu^\gamma(p_1) [p_1 \cdot (k_1 + k_2) g^{\mu\beta} - p_1^\beta (k_1 + k_2)^\mu] \bar{u}_l(k_2) \gamma_\beta v_l(k_1) \bar{u}_N(p_4) u_N(p_2)}{M^2 m_\pi [t_1 - m_\sigma^2 + im_\sigma \Gamma_\sigma] [m_\rho^2 - im_\rho \Gamma_\rho] [M^2 - m_\rho^2 + im_\rho \Gamma_\rho]} \quad (\text{A.16})$$

The squared invariant amplitude is then

$$|\overline{\mathcal{M}}|^2 = |\overline{\mathcal{M}_a + \mathcal{M}_b + \mathcal{M}_c + \mathcal{M}_d}|^2 + |\overline{\mathcal{M}_e}|^2 \quad (\text{A.17})$$

where

$$|\overline{\mathcal{M}_a}|^2 = \frac{F_\pi^2 A_\pi g_{\gamma\omega}^2 g_{\gamma\rho}^2 g_{\pi NN}^2 g_{\omega\rho\pi}^2}{[m_\omega^4 + m_\omega^2 \Gamma_\omega^2] [(M^2 - m_\rho^2)^2 + m_\rho^2 \Gamma_\rho^2]} \quad (\text{A.18})$$

$$|\overline{\mathcal{M}_b}|^2 = \frac{F_\pi^2 A_\pi g_{\gamma\rho}^2 g_{\gamma\omega}^2 g_{\pi NN}^2 g_{\omega\rho\pi}^2}{[m_\rho^4 + m_\rho^2 \Gamma_\rho^2] [(M^2 - m_\omega^2)^2 + m_\omega^2 \Gamma_\omega^2]} \quad (\text{A.19})$$

$$|\overline{\mathcal{M}_c}|^2 = \frac{F_\pi^2 A_\pi g_{\gamma\phi}^2 g_{\gamma\rho}^2 g_{\pi NN}^2 g_{\phi\rho\pi}^2}{[m_\phi^4 + m_\phi^2 \Gamma_\phi^2] [(M^2 - m_\rho^2)^2 + m_\rho^2 \Gamma_\rho^2]} \quad (\text{A.20})$$

$$|\overline{\mathcal{M}_d}|^2 = \frac{F_\pi^2 A_\pi g_{\gamma\rho}^2 g_{\gamma\phi}^2 g_{\pi NN}^2 g_{\phi\rho\pi}^2}{[m_\rho^4 + m_\rho^2 \Gamma_\rho^2] [(M^2 - m_\phi^2)^2 + m_\phi^2 \Gamma_\phi^2]} \quad (\text{A.21})$$

$$\begin{aligned}
\text{Re } \overline{\mathcal{M}_a^* \mathcal{M}_b} &= \frac{F_\pi^2 A_\pi g_{\gamma\omega}^2 g_{\gamma\rho}^2 g_{\pi NN}^2 g_{\omega\rho\pi}^2}{[m_\omega^4 + m_\omega^2 \Gamma_\omega^2][(M^2 - m_\rho^2)^2 + m_\rho^2 \Gamma_\rho^2][m_\rho^4 + m_\rho^2 \Gamma_\rho^2][(M^2 - m_\omega^2)^2 + m_\omega^2 \Gamma_\omega^2]} \\
&\times \left[(m_\omega^2 m_\rho^2 + m_\omega m_\rho \Gamma_\omega \Gamma_\rho) \{ (M^2 - m_\rho^2)(M^2 - m_\omega^2) + m_\omega m_\rho \Gamma_\omega \Gamma_\rho \} \right. \\
&\quad \left. - (m_\rho^2 m_\omega \Gamma_\omega - m_\omega^2 m_\rho \Gamma_\rho) \{ (M^2 - m_\omega^2) m_\rho \Gamma_\rho - (M^2 - m_\rho^2) m_\omega \Gamma_\omega \} \right]
\end{aligned} \tag{A.22}$$

$$\begin{aligned}
\text{Re } \overline{\mathcal{M}_a^* \mathcal{M}_c} &= \frac{F_\pi^2 A_\pi g_{\gamma\omega} g_{\gamma\phi} g_{\gamma\rho}^2 g_{\pi NN}^2 g_{\omega\rho\pi} g_{\phi\rho\pi}}{[m_\omega^4 + m_\omega^2 \Gamma_\omega^2][(M^2 - m_\rho^2)^2 + m_\rho^2 \Gamma_\rho^2][m_\phi^4 + m_\phi^2 \Gamma_\phi^2]} \\
&\times \left[(m_\omega^2 m_\phi^2 + m_\omega m_\phi \Gamma_\omega \Gamma_\phi) \{ (M^2 - m_\rho^2)^2 + m_\rho^2 \Gamma_\rho^2 \} \right]
\end{aligned} \tag{A.23}$$

$$\begin{aligned}
\text{Re } \overline{\mathcal{M}_a^* \mathcal{M}_d} &= \frac{F_\pi^2 A_\pi g_{\gamma\omega} g_{\gamma\phi} g_{\gamma\rho}^2 g_{\pi NN}^2 g_{\omega\rho\pi} g_{\phi\rho\pi}}{[m_\omega^4 + m_\omega^2 \Gamma_\omega^2][(M^2 - m_\rho^2)^2 + m_\rho^2 \Gamma_\rho^2][m_\rho^4 + m_\rho^2 \Gamma_\rho^2][(M^2 - m_\phi^2)^2 + m_\phi^2 \Gamma_\phi^2]} \\
&\times \left[(m_\omega^2 m_\rho^2 + m_\omega m_\rho \Gamma_\omega \Gamma_\rho) \{ (M^2 - m_\rho^2)(M^2 - m_\phi^2) + m_\rho m_\phi \Gamma_\rho \Gamma_\phi \} \right. \\
&\quad \left. - (m_\rho^2 m_\omega \Gamma_\omega - m_\omega^2 m_\rho \Gamma_\rho) \{ (M^2 - m_\phi^2) m_\rho \Gamma_\rho - (M^2 - m_\rho^2) m_\phi \Gamma_\phi \} \right]
\end{aligned} \tag{A.24}$$

$$\begin{aligned}
\text{Re } \overline{\mathcal{M}_b^* \mathcal{M}_c} &= \frac{F_\pi^2 A_\pi g_{\gamma\omega} g_{\gamma\phi} g_{\gamma\rho}^2 g_{\pi NN}^2 g_{\omega\rho\pi} g_{\phi\rho\pi}}{[m_\rho^4 + m_\rho^2 \Gamma_\rho^2][(M^2 - m_\rho^2)^2 + m_\rho^2 \Gamma_\rho^2][m_\phi^4 + m_\phi^2 \Gamma_\phi^2][(M^2 - m_\omega^2)^2 + m_\omega^2 \Gamma_\omega^2]} \\
&\times \left[(m_\rho^2 m_\phi^2 + m_\rho m_\phi \Gamma_\rho \Gamma_\phi) \{ (M^2 - m_\omega^2)(M^2 - m_\rho^2) + m_\omega m_\rho \Gamma_\omega \Gamma_\rho \} \right. \\
&\quad \left. - (m_\rho^2 m_\phi \Gamma_\phi - m_\phi^2 m_\rho \Gamma_\rho) \{ (M^2 - m_\omega^2) m_\rho \Gamma_\rho - (M^2 - m_\rho^2) m_\omega \Gamma_\omega \} \right]
\end{aligned} \tag{A.25}$$

$$\begin{aligned}
\text{Re } \overline{\mathcal{M}_b^* \mathcal{M}_d} &= \frac{F_\pi^2 A_\pi g_{\gamma\omega} g_{\gamma\phi} g_{\gamma\rho}^2 g_{\pi NN}^2 g_{\omega\rho\pi} g_{\phi\rho\pi}}{[m_\rho^4 + m_\rho^2 \Gamma_\rho^2][(M^2 - m_\omega^2)^2 + m_\omega^2 \Gamma_\omega^2][(M^2 - m_\phi^2)^2 + m_\phi^2 \Gamma_\phi^2]} \\
&\times \left[(M^2 - m_\omega^2)(M^2 - m_\phi^2) + m_\omega m_\phi \Gamma_\omega \Gamma_\phi \right]
\end{aligned} \tag{A.26}$$

$$\begin{aligned}
\text{Re } \overline{\mathcal{M}_c^* \mathcal{M}_d} &= \frac{F_\pi^2 A_\pi g_{\gamma\phi}^2 g_{\gamma\rho}^2 g_{\pi NN}^2 g_{\phi\rho\pi}^2}{[m_\rho^4 + m_\rho^2 \Gamma_\rho^2][(M^2 - m_\rho^2)^2 + m_\rho^2 \Gamma_\rho^2][m_\phi^4 + m_\phi^2 \Gamma_\phi^2][(M^2 - m_\phi^2)^2 + m_\phi^2 \Gamma_\phi^2]} \\
&\times \left[(m_\rho^2 m_\phi^2 + m_\rho m_\phi \Gamma_\rho \Gamma_\phi) \{ (M^2 - m_\rho^2)(M^2 - m_\phi^2) + m_\rho m_\phi \Gamma_\rho \Gamma_\phi \} \right. \\
&\quad \left. - (m_\rho^2 m_\phi \Gamma_\phi - m_\phi^2 m_\rho \Gamma_\rho) \{ (M^2 - m_\phi^2) m_\rho \Gamma_\rho - (M^2 - m_\rho^2) m_\phi \Gamma_\phi \} \right]
\end{aligned} \tag{A.27}$$

$$|\mathcal{M}_e|^2 = \frac{F_\sigma^2 A_\sigma g_{\gamma\rho}^4 g_{\sigma NN}^2 g_{\sigma\rho\rho}^2}{[m_\rho^4 + m_\rho^2 \Gamma_\rho^2][(M^2 - m_\rho^2)^2 + m_\rho^2 \Gamma_\rho^2]} \tag{A.28}$$

with

$$A_\pi = -\frac{2\pi\alpha}{M^2} \frac{[t_2^2 + (t_2 - t_1 + M^2)^2] t_1}{m_\pi^2 [t_1 - m_\pi^2]^2}, \quad A_\sigma = \frac{8\pi\alpha}{M^2} \frac{[t_2^2 + (t_2 - t_1 + M^2)^2] (4m_N^2 - t_1)}{m_\pi^2 [(t_1 - m_\sigma^2)^2 + m_\sigma^2 \Gamma_\sigma^2]},$$

and

$$F_\pi = \left[\frac{\Lambda_\pi^2 - m_\pi^2}{\Lambda_\pi^2 - t_1} \right] \left[\frac{m_\rho^2 - m_\pi^2}{m_\rho^2 - t_1} \right], \quad F_\sigma = \left[\frac{\Lambda_\sigma^2 - m_\sigma^2}{\Lambda_\sigma^2 - t_1} \right] \left[\frac{\Lambda_{\sigma\rho\rho}^2 - m_\rho^2}{\Lambda_{\sigma\rho\rho}^2 - t_1} \right].$$

- [1] CERES collaboration, G. Agakishiev *et al.*, Phys. Lett. **422**, 405 (1998).
- [2] HELIOS-3 Collaboration, M. Masera *et al.*, Nucl. Phys. **A590**, 93c (1995); NA50 Collaboration, E Scomparin *et al.*, *ibid* **A610**, 331c (1996).
- [3] G. Q. Li, C. M. Ko and G. E. Brown, Phys. Rev. Lett. **75**, 4007 (1995).
- [4] W. Cassing, W. Ehchalt and C. M. Ko, Phys. Lett. **B363**, 35 (1995).
- [5] R. Rapp, G. Chanfray and J. Wambach, Nucl. Phys. **A617**, 472 (1997).
- [6] W. Cassing, E. L. Bratkovskaya, R. Rapp and J. Wambach, Phys. Rev. **C57**, 916 (1998).
- [7] B. Friman and H. J. Pirner, Nucl. Phys. **A617**, 496 (1997).
- [8] F. Klingl, H. Kaiser and W. Weise, Nucl. Phys. **A624**, 527 (1997).
- [9] H. Shiomi and T. Hatsuda, Phys. Lett. **B 334**, 281 (1994).
- [10] J. Alam, S. Sarkar, P. Roy, T. Hatsuda and B. Sinha, Ann. Phys. (NY) **286**, 159 (2000).
- [11] A. Bhattacharyya, S. K. Ghosh and S. Raha, Phys. Rev. **C60**, 018202 (1999).
- [12] K. Ozawa *et al.*, Phys. Rev. Lett. **86**, 5019 (2001).
- [13] N. Bianchi *et al.*, Phys. Rev. **C54**, 1688 (1996).
- [14] V. Muccifora *et al.*, Phys. Rev. **C60**, 064616 (1999).
- [15] N. Bianchi, E. De Sanctis, M. Mirazita and V. Muccifora, Phys. Rev. **C60**, 064617 (1999).
- [16] T. Falter, S. Leupold and U. Mosel, Phys. Rev. **C62**, 031602(R) (2000).
- [17] R. J. Glauber, in *Lectures in Theoretical Physics*, edited by W. E. Brittin and L. G. Dunham (Wiley Interscience, New York, 1959), Vol. I, p. 315.
- [18] R. J. Glauber, in *High Energy Physics and Nuclear Structure*, edited by S. Devons (Plenum, New York, 1970), p. 207.
- [19] D. R. Yennie, in *Hadronic Interactions of Electrons and Photons*, edited by J. Cummings and H. Osborn (Academic, New York/London, 1971), p. 321.
- [20] T. H. Bauer, R. D. Spital and D. R. Yennie, Rev. Mod. Phys. **50**, 261 (1978).
- [21] T. Falter, S. Leupold and U. Mosel, Phys. Rev. **C64**, 024608 (2001).
- [22] J. Alam, S. K. Ghosh, P. Roy and S. Sarkar, Phys. Rev. C **66**, 042202(R) (2002).
- [23] G. J. Lolos *et al.*, Phys. Rev. Lett. **80**, 241 (1998); G. M. Huber *et al.*, Phys. Rev. Lett. **80**, 5285 (1998).
- [24] S. D. Drell and J. D. Walecka, Ann. Phys. NY, **28** 18 (1964).
- [25] M. Soyeur, Nucl. Phys. **A 606**, 237 (1996).
- [26] PAC20 jeopardy proposal G7 experiment (originally E94-002).
- [27] R. P. Feynman, Photon-hadron interactions, W. A. Benjamin, Inc., Massachusetts, 1972.
- [28] J. H. Weis, Acta. Phys. Pol. **B7**, 851 (1976).
- [29] G. Piller and W. Weise, Phys. Rep. **330** 1 (2000).
- [30] J. J. Sakurai, Currents and Mesons, Univ. of Chicago Press, Chicago, 1969.
- [31] G. E. Brown and M. Rho, Phys. Rev. Lett. **66**, 2720 (1991).
- [32] T. Hatsuda and S. H. Lee Phys. Rev. **C 46**, R34 (1992).
- [33] K. Saito, A. W. Thomas and K. Tsushima, Phys. Rev. **C 56**, 566 (1997).
- [34] B. D. Serot and J. D. Walecka, Adv. Nucl. Phys. **16**, Plenum, New York, 1986.
- [35] T. Hatsuda, H. Shiomi and H. Kuwabara, Prog. Th. Phys. **95**, 1009 (1996).
- [36] H. Kuwabara and T. Hatsuda, Prog. Th. Phys. **94**, 1163 (1995).
- [37] V. N. Gribov, Zh. Eksp. Teor. Fiz. **57**, 1306 (1969) JETP **30**, 709 (1970).
- [38] A. Pautz and G. Shaw, Phys. Rev. **C57**, 2648 (1998).
- [39] K. J. Eskola, R. Vogt and X. N. Wang, Int. J. Mod. Phys. **A10**, 3087 (1995).
- [40] D. W. G. S. Leith, in Electromagnetic Interactions of Hadrons, Ed. A. Donnachie and G. Shaw, Plenum Pub. Co. 1977.
- [41] B. Friman and M. Soyeur, Nucl. Phys. **A600**, 477 (1996).
- [42] M. Effenberger, E. L. Bratkovskaya and U. Mosel, Phys. Rev. **C60**, 044614 (1999).
- [43] N. M. Kroll, T. D. Lee and B. Zumino, Phys. Rev. **157**, 1376 (1967).
- [44] Particle Data Group, R.M. Barnett *et al.*, Phys. Rev. **D54**, 1(1996).
- [45] M. Gell-Mann, D. Sharp and W. D. Wagner, Phys. Rev. Lett. **8**, 261 (1962).
- [46] L. A. Kondratyuk, M. I. Krivoruchenko, N. Bianchi, E. De Sanctis and V. Muccifora, Nucl. Phys. **A 579** 453 (1994).
- [47] L. A. Kondratyuk, A. Sibirtsev, W. Cassing, Ye. S. Golubeva and M. Effenberger, Phys. Rev. **C 58**, 1078 (1998).
- [48] H. A. Weldon, Ann. Phys. **228**, 43 (1993).
- [49] S. J. Wallace, Phys. Rev. **12**, 179 (1975).
- [50] E. Byckling and K. Kajantie, Particle Kinematics, John Wiley and Sons, 1973.